Journal of MATERIALS RESEARCH

Article
DOI: 10.1557/jmr.2018.447

(NANO)MATERIALS FOR BIOMEDICAL APPLICATIONS

FOCUS ISSUE

Development of multilayered biomimetic bone plates: In vitro release assessment

R. Seda Tığlı Aydın[1,a] Seda Uyanık[2]

[1]Department of Biomedical Engineering, Bülent Ecevit University, İncivez-Zonguldak 67100, Turkey; and Department of Nanotechnology Engineering, Bülent Ecevit University, İncivez-Zonguldak 67100, Turkey
[2]Department of Nanotechnology Engineering, Bülent Ecevit University, İncivez-Zonguldak 67100, Turkey
[a)]Address all correspondence to this author. e-mail: rseda.tigli@gmail.com, seda.aydin@beun.edu.tr

Received: 5 September 2018; accepted: 7 November 2018

In this study, Sr-incorporated nano-assembled hydroxyapatite structures (HASr) on 316L stainless steel bone plates were prepared by a biomimetic method induced by 10× simulated body fluid (SBF). First, HASr was coated on bone plates by the interaction of ions with 10× SBF containing different concentration of strontium ions. Then, silver coating is achieved as a second layer on bone plates. The cumulative release of strontium ions (Sr^{2+}) and silver ions (Ag^{+}) from multilayered HASr-Ag bone plates at the end of 15 days was in the range of 0.016–0.085 mM and 0.064–0.135 mM, respectively. The release mechanism for the bone plates was evaluated by several mathematical models that best fit the release data. The results showed that Sr^{2+} and Ag^{+} are released from multilayered bone plates by diffusion, whereas the release of Ag^{+} is not occurred by diffusion, instead the mechanism is dissolution, when silver is coated alone on bone plates.

Introduction

Metallic implants (i.e., bone plates, screws, and Kirschner wire) have been widely used in orthopedic fields due to their significant mechanical properties and biocompatibility [1, 2]. However, bone bonding or osteoconductivity is still challenging for most clinical cases since the material-dependent factors (i.e., chemical bonding associated with structure of the material) play an important role in the tissue response [3, 4]. Thus, to overcome the failure at bone and implant interface, coating of bioactive ceramics on metallic implants is suggested by a variety of techniques, including plasma spraying, sol–gel, electrophoretic deposition, laser ablation, hydrothermal, and biomimetic methods [5, 6, 7, 8, 9, 10]. Among all these methods, biomimetic coating method is quite simple and cheap and has a low processing temperature with the ease of coating complex shapes [5]. In recent years, several studies reported that simulated body fluids (SBFs), a solution with ion concentrations and pH value similar to those of human plasma, provide a calcium-deficient (not stoichiometric) apatite layer grown on the surface of the implant [5, 7, 11, 12]. It is well known that biomimetic method produces hydroxyapatite (HA) coatings from SBF by precipitation of CaP at room temperature, which has been proven to enhance the cell proliferation and differentiation [13, 14]. Thus, the biomimetic layer coated implants are expected to develop bone bonding properties [15]. However, with this method, precipitation takes days to weeks due to the supersaturation levels in the SBF recipes, which commonly do not allow for rapid deposition rates. Thus, previous studies reported that synthesis of HA from supersaturated aqueous solutions like 10× SBF (10 times concentrated SBF) promoted the rapid deposition (2–24 h) of HA, which is advantageous due to low cost and simplicity [13, 15, 16].

Strontium has received a lot of interest due to its biological role in bone metabolism, by effectively promoting bone formation and reducing bone resorption [17, 18]. Although the main mechanism of strontium in bone-related cells has not been fully explored yet, previous studies have shown the effect of strontium on preosteoblastic cell replication, suggesting that Sr^{2+} ions activate the Wnt/β-catenin signaling pathway, which stimulates osteogenesis and differentiation into osteoblasts [19, 20, 21, 22]. Thus, Sr^{2+} is announced as a promising enhancer of bone-related implants, and recently, studies were performed for the development of strontium-substituted HA ceramics, which are used for coatings [23, 24]. Due to the similar chemical properties of Ca^{2+} and Sr^{2+}, Sr^{2+} can be easily

https://doi.org/10.1557/jmr.2018.447 Published online by Cambridge University Press

© Materials Research Society 2019

introduced as a natural substitute for calcium in HA, and strontium-incorporated HA (HASr) coatings have been successfully obtained using several methods, such as biomimetic precipitation, plasma spray, co-deposition sputter, and pulsed laser deposition [19, 20, 23, 24]. Coating of implants is not only motivated by the development of bone bonding or osteoconductivity but also being extensively investigated to avoid bacterial proliferation and biofilm formation, which lead to endoprosthesis infections [25, 26]. Hence, silver-coated implants are suggested due to the well-known antimicrobial activity of silver [27–30].

Recently, a few studies have reported dual coating of strontium and silver in HA on titanium implants [31]. Fielding et al. have incorporated Ag_2O and SrO into plasma-sprayed HA coatings [31]. Huang et al. investigated silver- and strontium-doped HA coatings on titanium nanotubes

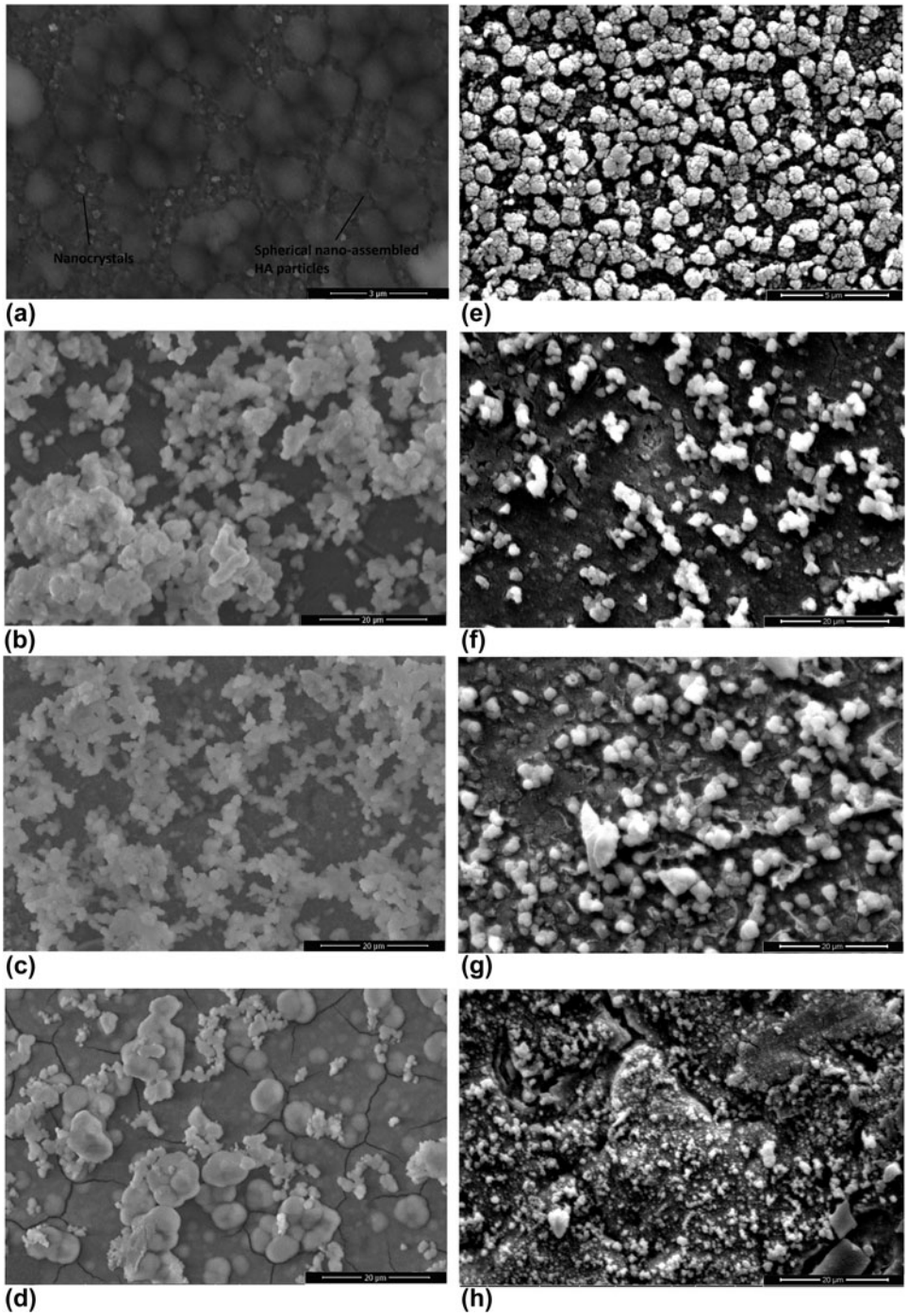


Figure 1: SEM images of (a) HA, (b) HASr1, (c) HASr2, (d) HASr3, (e) HA-Ag, (f) HASr1-Ag, (g) HASr2-Ag, and (h) HASr3-Ag coatings on 316L SS bone plates.

https://doi.org/10.1557/jmr.2018.447 Published online by Cambridge University Press

© Materials Research Society 2019

fabricated by electrodeposition and reported suitability of the biomaterial for orthopedic applications [32]. Geng et al. successfully prepared silver- and strontium-incorporated HA coatings on Ti, which were fabricated via one-step hydrothermal method [33]. However, according to our knowledge, there is no available information on providing HASr coatings on 316L stainless steel (316L SS) bone plates using biomimetic method induced by concentrated SBF-like solutions (10× SBF), and there is no available information of the ion release mechanism.

Nanomaterials not only would offer several advantages over conventional drug therapies but also expected to overcome side effects of dosing and toxicity. In this study, first, it is aimed to achieve multilayered form of strontium-incorporated and silver-coated bone-like nano-assembled apatite coatings on 316L SS bone plates, which can provide successful bone–implant interaction without causing implant infection in clinical applications. The significance and originality of this study arise from the fact that multilayered HA coatings sometimes fail efficient ion release for the osteogenesis or antimicrobial activity of the implanted area, and therefore, the release mechanisms should be determined. This study is motivated by the need to investigate release kinetics of Sr^{2+} and Ag^{+} from multilayered biomimetic bones plates due to safety concerns (i.e., possible side effects) associated with the long-term application of strontium and silver in local application. Therefore, investigation of the release profiles of Sr^{2+} and Ag^{+} is the intention of this study by researching mathematical models to evaluate release mechanisms.

In the present study, first, HASr coatings on 316L SS bone plates were maintained via a simple, cheap, time-reducing, and efficient biomimetic method with 10× SBF, then silver is coated as a second layer. The morphological, surface, and physicochemical properties of the coatings were subsequently investigated and analyzed. The coated layers are reservoirs of Sr^{2+} and Ag^{+}, and the release mechanisms are determined according to several mathematical methods.

Results and discussion

In this study, it is aimed to enhance the biological and chemical properties of HA by incorporating strontium to produce HASr

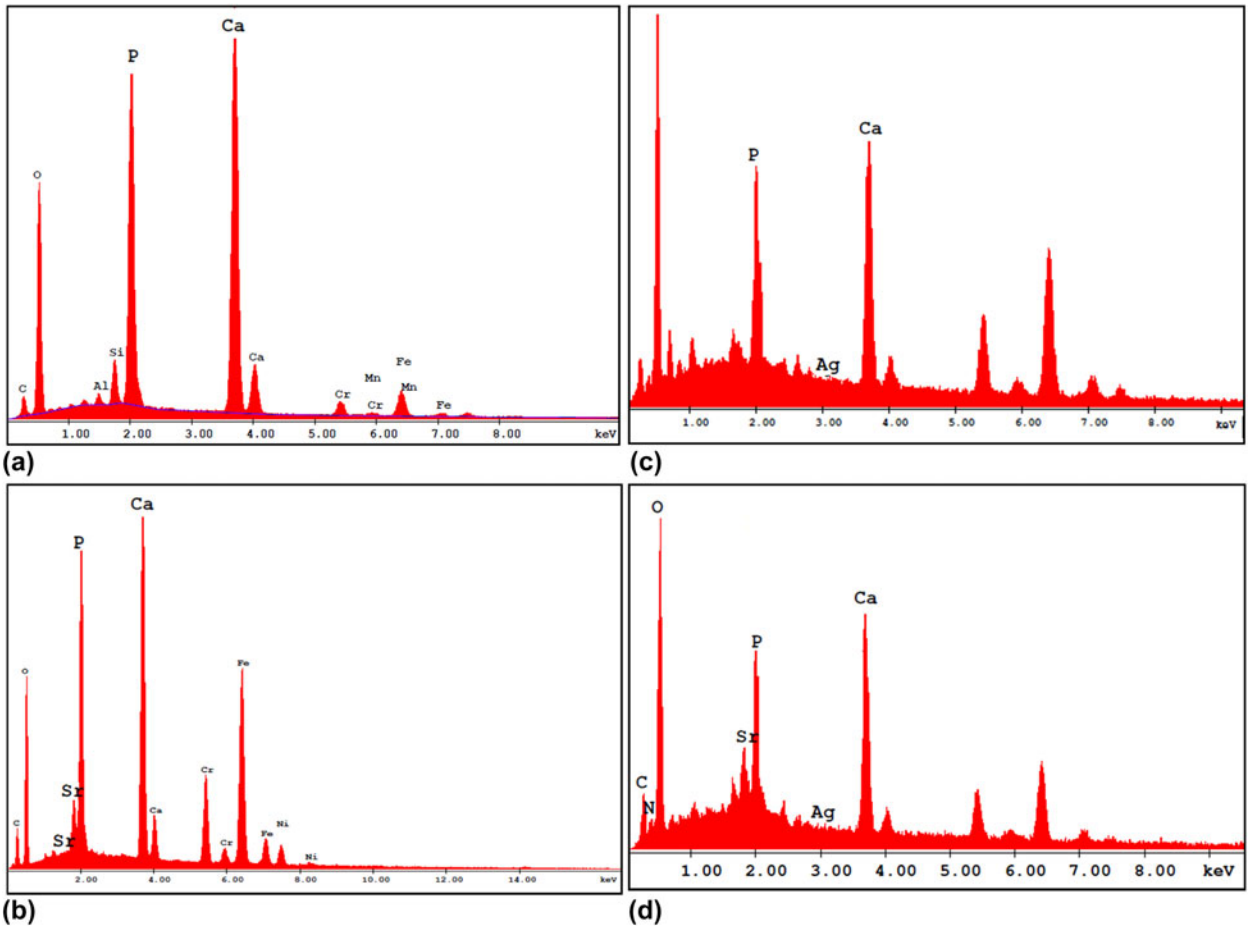


Figure 2: EDAX spectra of (a) HA, (b) HASr, (c) HA-Ag, and (d) HASr-Ag coatings.

https://doi.org/10.1557/jmr.2018.447 Published online by Cambridge University Press

© Materials Research Society 2019

coatings. Then, Ag was added to biomimetic coating, as a second layer, to produce HASr-Ag coatings on 316L SS bone plates. In the present study, we used modified recipe of 10× SBF, developed previously [13], to synthesize HASr biomimetic coatings, which could support bone growth more than pure HA does [39]. Thus, not only Sr was incorporated into the HA structure by biomimetic method, but also 316L SS bone plates were coated with Sr-doped HA and Ag by means of multilayer coatings. However, previously it was reported that an alkali pretreatment is essential to establish and induce a bioactive HA layer on the surface of 316L SS [7]. Thus, 316L SS bone plates were first alkali treated to form an amorphous sodium chrome pickle layer as an inter-compound for ceramic and metal linkage [7].

Morphological observation

The surface morphology of HA coatings on bone plates was observed by SEM given in Fig. 1. During precipitation by 10× SBF biomimetic approach, ions in the SBF tend to form nanosized amorphous calcium phosphate precursors. After nano-HA crystals are formed, the growth of apatites continues through these nucleation zones and particles came together to form micrometer-sized spherical nanoaggregates [15]. As

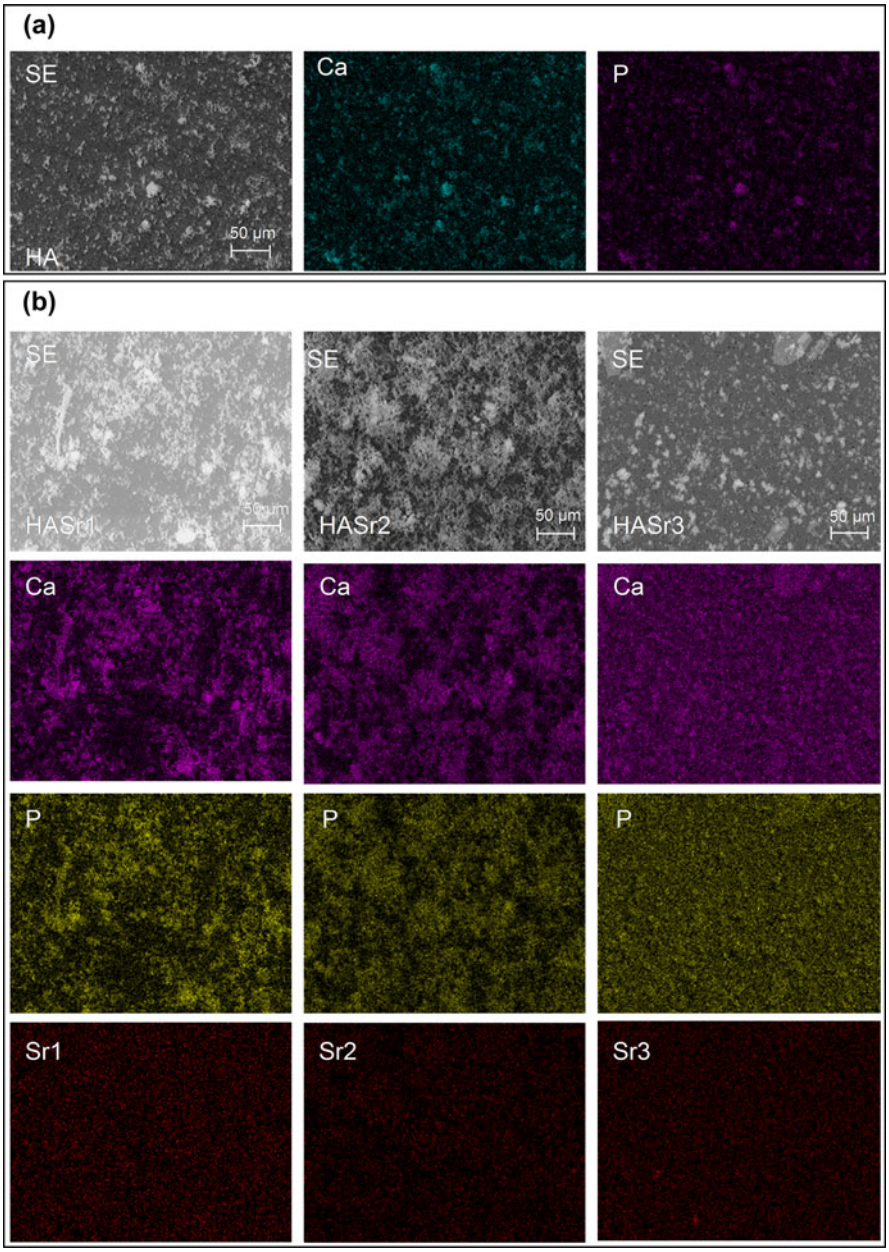


Figure 3: Elemental mapping of (a) HA and (b) HASr coatings and distributions of individual elements based on selected region of the sample.

https://doi.org/10.1557/jmr.2018.447 Published online by Cambridge University Press

© Materials Research Society 2019

shown in Figs. 1(a) and 1(b), nano-assembled HA structures (cauliflower structure) are formed as uniform aggregates (0.5–2 μm). Although the same morphologies were observed on HASr coatings [Figs. 1(b)–1(d)], HA clusters were nonuniform aggregates. Moreover, as shown in Fig. 1(d), it was observed that HA clusters were much more irregular in HASr3 coatings than in other coatings, forming large clusters away from nano-patterns. This result may be due to the Ca/P molar ratio (1.16, which was determined by XRF analysis) of apatites formed compared to Ca/P molar ratio of stoichiometric HA (1.67) [15]. HA morphologies in HA-Ag coatings were observed to be intact [Figs. 1(e)–1(h)]. Especially, the bright areas indicate the presence of silver coating.

EDAX analysis and elemental mapping

Figure 2 shows the spectra obtained from HA, HASr, HA-Ag, and HASr-Ag coatings on bone plates. The Sr and Ag peaks [Figs. 2(b)–2(d)] in the spectra confirmed the presence of Sr and Ag, incorporated successfully into the structure. The Ca/P molar ratio provides information on phase purity, chemical homogeneity, and solubility of a material to be used as bone therapeutics. Human bone contains 34.8 wt% Ca and 15.2 wt% P ions and the Ca/P molar ratio is about 1.77. However, the stoichiometric HA contains 39.8 wt% Ca and 18.5 wt% P and its Ca/P molar ratio is about 1.67 [15, 16]. Using EDAX analysis, the Ca/P molar ratios of HA, HASr2, HA-Ag, and HASr2-Ag coatings were found to be 1.64, 1.60, 1.36, and 1.58, respectively. However, since EDAX analysis can be performed from only certain regions of the samples, the reliability of the results is controversial. Thus, the Ca/P molar ratios are determined again by the XRF analysis, described in section "XRD and XRF results". Moreover, Ag contents in the HA-Ag and HASr2-Ag coatings were 0.13% and 0.16% by weight, respectively. The Sr contents in HASr2 and HASr2-Ag coatings were found to be 4.58% and 4.43% by weight, respectively.

The distribution and homogeneity of Ca, P, Sr, and Ag in HA coatings were observed by elemental mapping method combined with EDAX analysis. Figures 3(a), 3(b), and 4 represent elemental mapping of HA, HASr, and HA-Ag coatings through selected regions, respectively. As shown in Fig. 3 (a), Ca and P are homogenously distributed and clustered in the same regions. In the case of Sr-incorporated coatings, Sr is located on Ca/P nuclei, which carry HA aggregates, and has been found to participate in the structure through these regions homogenously [Fig. 3(b)]. However, Ag was observed to be not only homogenously distributed on Ca/P nuclei regions but also distributed uniformly throughout the structure (Fig. 4).

Raman spectroscopy

In Fig. 5, Raman spectra obtained from all types of Sr-incorporated HA coatings are compared with those of HA coatings according to the detected Raman spectroscopic bands and their assignments. In the spectrum of HA [Fig. 5(a)], an intense band situated around 962 cm^{-1} is assigned to P–O symmetric stretching mode (ν_1) of the PO_4 group, representing the most characteristic band of carbonated apatites [40, 41]. The bands at 428 cm^{-1} and 589 cm^{-1} correspond to the ν_2

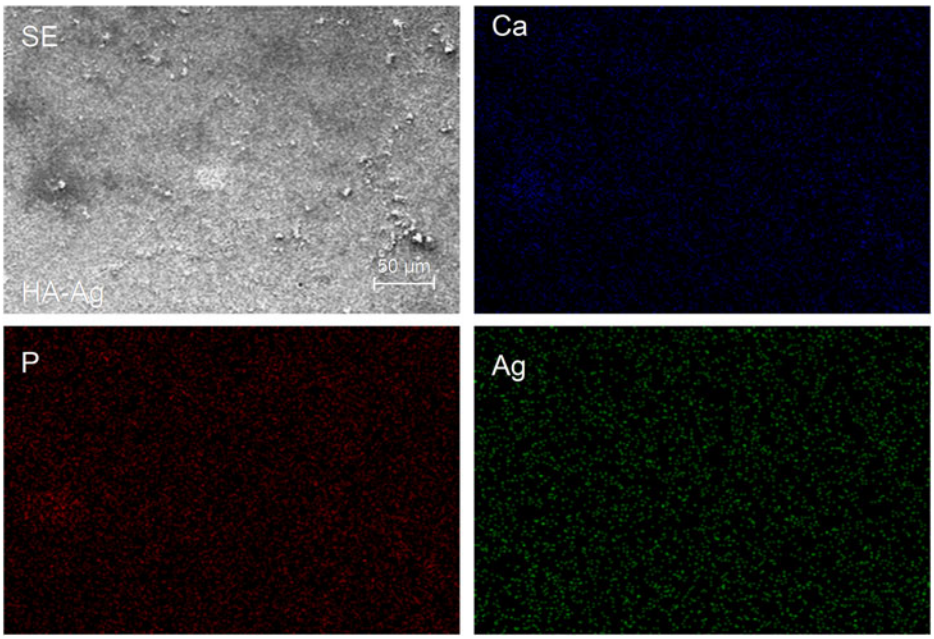


Figure 4: Elemental mapping of HA-Ag coatings and distributions of individual elements based on selected region of the sample.

https://doi.org/10.1557/jmr.2018.447 Published online by Cambridge University Press

© Materials Research Society 2019

bending vibration and ν_4 mode of the PO_4 group, respectively [16]. A shift of stretching mode (ν_1) of the PO_4 group from 962 to 959 cm^{-1} is observed for HASr coatings [Figs. 5(b)–5(d)] with Sr incorporation to HA structure. This downshifting of the ν_1 phosphate band to slightly lower values is due to the substitution of Ca by Sr in the apatite structure [41, 42]. The band shift correlates with the progressing Sr substitution, indicating increased Sr incorporation except in HASr3. O'Donnell et al. detected down-shifting of Raman bands of phosphate groups for modes ν_1, ν_2, and ν_4, with increasing Sr and decreasing Ca content [43], which is in a good correlation with our results.

XRD and XRF results

XRD patterns of HA, HASr, and HA-Ag coatings are given in Fig. 6 to determine phase purity and structure of HA coatings. The peaks observed at $2\theta = 26°$ and 32° are the characteristic peaks of HA [15]. The presence of wide peaks in the spectra indicates the amorphous HA structure, which is analogous to

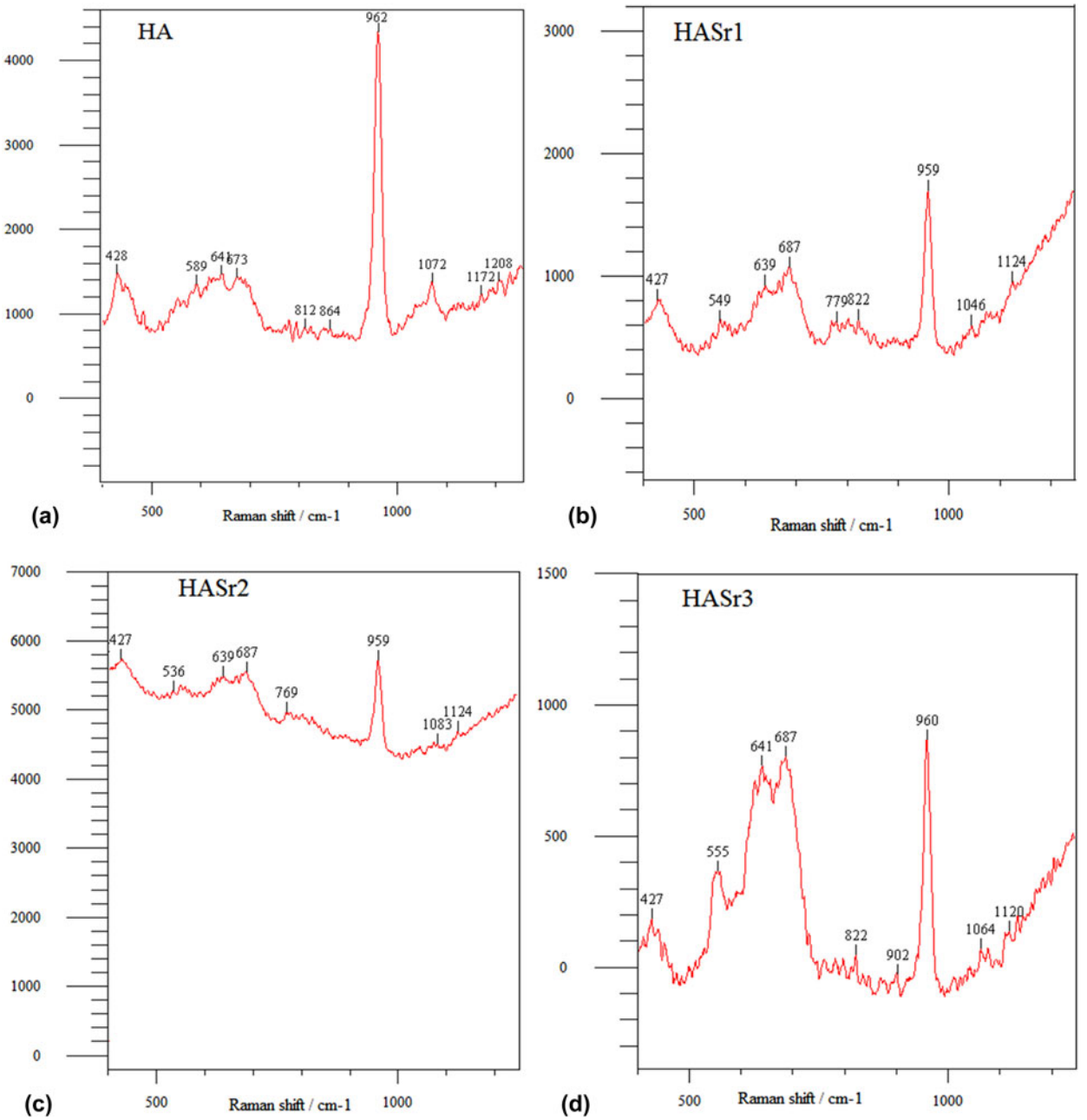


Figure 5: Raman spectra of (a) HA, (b) HASr1, (c) HASr2, and (d) HASr3 coatings.

https://doi.org/10.1557/jmr.2018.447 Published online by Cambridge University Press

© Materials Research Society 2019

the crystallographic behavior of the biological apatite pattern [44]. As shown in Fig. 6, there are no differences in diffraction peaks between XRD patterns of HA and HASr, which indicates that there are no extraneous phases, such as dicalcium phosphate anhydrous, dicalcium phosphate dihydrate, and β-tricalcium phosphate, and only monolayer in HA structure. These results indicated that incorporation of Sr into HA structure did not affect the biomimetic HA, which conclude the suitability of biomimetic method for the production of HASr. However, the peak intensity is increased (peak at 26°) with Sr addition [Fig. 6(b)]. This result can be attributed to the fact that Sr is heavier and contains more electrons than Ca, which is consistent with the literature [43]. Therefore, an increase in crystallinity of HA structure has occurred with Sr substitution. The XRD spectrum of HA-Ag coatings is similar to that of HA, but the peak intensities slightly increased and the 2θ values slightly shifted downward [Fig. 6(c)]. This shift can be explained by the change in the crystal sizes of the particles as a result of heat treatment after Ag coating [30]. The XRD of HA-Ag also demonstrates that Ag coating as a second layer on biomimetic bone plates still exhibit the apatite characteristics with good crystal structure and no new phase or impurity.

The amounts of strontium and silver within the biomimetic coatings on bone plates and Ca/P ratios were determined by XRF analysis and the results are demonstrated in Table I. Ca/P ratios of HA, HA-Ag, HASr1-Ag, HASr2-Ag, and HASr3-Ag coatings were found to be 1.64, 1.65, 1.63, 1.59, and 1.16, respectively. The results revealed that the amounts of measured Sr within HASr1-Ag, HASr2-Ag, and HASr3-Ag coatings were 0.4, 0.8, and 1.0 mM, respectively. It has been well studied that Sr substitution in HA has a superior effect both in vitro and in vivo, enhancing osteoblast proliferation and differentiation [45, 46, 47]. Moreover, Sr dose control over cells positively influences proliferation and osteogenic differentiation of cells in vitro, which is reported to be most effective between 0.001 and 1 mM [41, 48, 49]. Our results are in the range of the doses reported that positively influence proliferation and osteogenic differentiation of cells. Although, Sr has also been implicated in antimicrobial activity [50], it has been well known that silver exhibits good antibacterial activity toward mammalian cell [26]. Previously, in vitro silver ion effects with the antibacterial activity against *Staphylococcus epidermidis*, which is the most common microorganism responsible for implant infections, have been investigated, and minimum inhibitory concentration

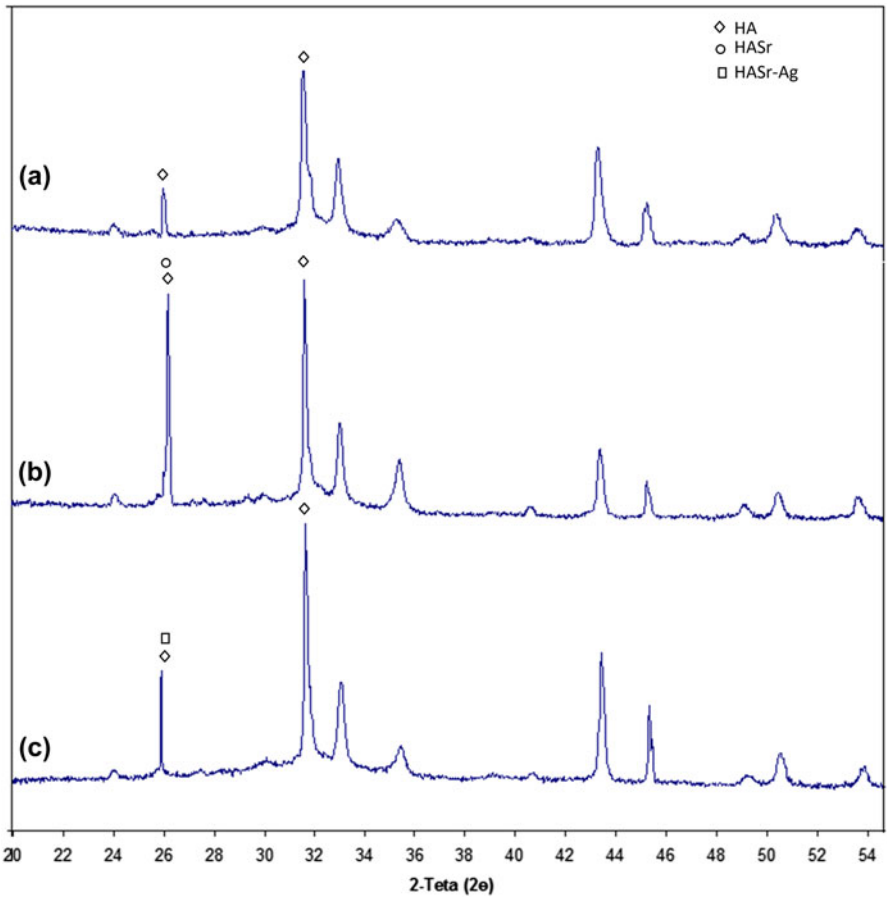


Figure 6: XRD spectra of (a) HA, (b) HASr, and (c) HASr-Ag coatings.

https://doi.org/10.1557/jmr.2018.447 Published online by Cambridge University Press

© Materials Research Society 2019

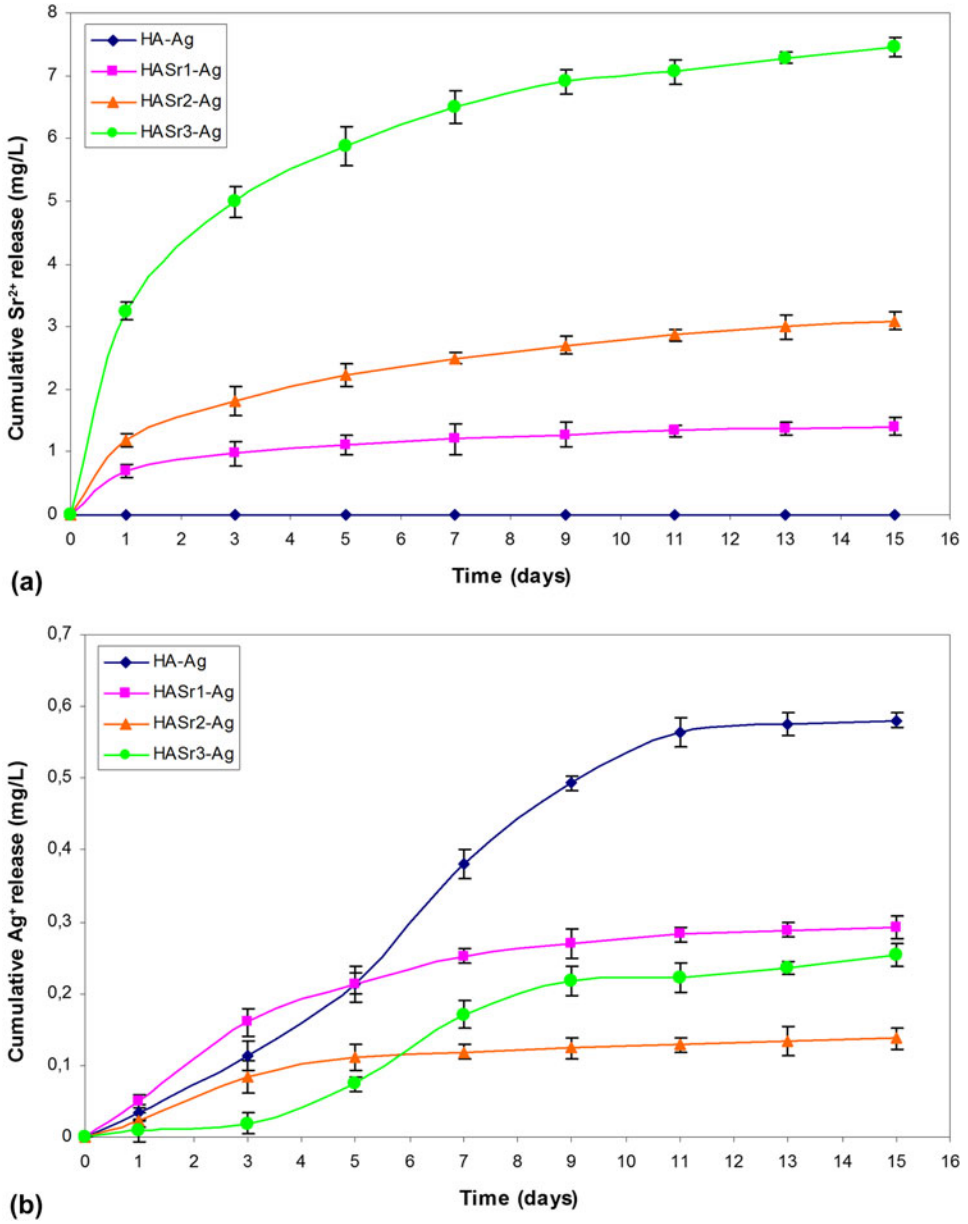


Figure 7: Cumulative release profiles of (a) Sr^{2+} and (b) Ag^{+} from HA-Ag, HASr1-Ag, HASr2-Ag, and HASr3-Ag bone plates.

(MIC) for silver ion was reported as 0.094 mM (~10 ppm) [25]. The measured silver amounts determined from XRF results within HA coatings were in the range of 24–29 ppm (Table I), which confirms the previously reported effective doses against implant infections [25].

TABLE I: XRF analysis of biomimetic coatings showing Ca/P ratio and Sr and Ag amounts.

Coating	Ca/P	Sr (ppm)	Ag (ppm)
HA	1.64	0	0
HA-Ag	1.65	0	29.485
HASr1-Ag	1.63	673.812	27.629
HASr2-Ag	1.59	1405.454	25.664
HASr3-Ag	1.16	1726.294	24.360

Release study of strontium and silver ions and mathematical modeling

The release of Sr^{2+} and Ag^{+} ions into PBS medium was determined via ICP-OES by analyzing the supernatants of HA-Ag, HASr1-Ag, HASr2-Ag, and HASr3-Ag bone plates during 15 days of incubation (Fig. 7). Figure 7(a) represents cumulative in vitro release profiles of Sr^{2+} and Ag^{+} ions. Measurements revealed that the amount of Sr^{2+} ions released was 0.008 mM (HASr1-Ag), 0.014 mM (HASr2-Ag), and 0.037 mM (HASr3-Ag) at day 1, and 0.016 mM (HASr1-Ag),

https://doi.org/10.1557/jmr.2018.447 Published online by Cambridge University Press

© Materials Research Society 2019

0.035 mM (HASr2-Ag), and 0.085 mM (HASr3-Ag) at day 15. Although all bone plates exhibited similar controlled release profiles, a significant burst release of Sr^{2+} was determined for HASr3-Ag. Based on the incorporated strontium amount, according to the XRF data, the total amounts of strontium released from the HASr1-Ag, HASr2-Ag, and HASr3-Ag bone plates at the end of 15 days were determined to be 10.5%, 11.0%, and 21.6%, respectively. This study is highly motivated to adapt a defined Sr^{2+} concentration at the defect site. Thus, this would be a great interest for clinical applications to generate a sustained and controlled release of Sr^{2+} ions in therapeutically relevant concentrations. The mechanism behind osteogenic proliferation, differentiation, and bone matrix formation with the usage of strontium lies on that fact that Sr^{2+} ions activate the Wnt/β-catenin pathway via calcium-sensing receptors [51]. The rationale behind this proposal is still unknown; however, the interaction of osteoblasts and Sr^{2+} ion plays an important role in the bone cell signaling with a concentration between 0.001 and 1 mM, which is reported as favorable for bone defect therapies [41, 48, 49]. The results obtained from release studies are in a good parallel with the previously reported doses (between 0.001 and 1 mM), which effects proliferation and osteogenic differentiation of cells [41, 48]. Moreover, after 15 days of incubation, the released doses of Sr^{2+}, which were still in the range of the doses, positively influence cells.

To reduce the risk of implant infections in orthopedic surgery, antimicrobial coatings, i.e., silver-coated implants, are attractive options for perioperative implant infections [52]. The most common technique to incorporate silver within HA coatings is dip-coating method of HA coatings into $AgNO_3$ for a period of time [28]. However, this method has the limitation of quick depletion of silver in vivo/in vitro, which may be due to the fact that silver resides on the outer surface of the coating. Thus, for long-term bacterial effect, a sustained release of silver is suggested for implant systems. Although silver-coated implants have great interest in clinical practice, it has been known that Ag^+ release may accumulate in the liver, kidney, and brain [53]. Moreover, the accumulation of ionic silver in the peri-implant tissue at unknown concentrations may affect the viability and differentiation of osteoblasts and osteoclasts [25]. Thus, in this study, the release of silver ions was determined by ICP-OES and the in vitro cumulative Ag^+ ion release profiles are demonstrated in Fig. 7(b). Ag^+ ion release was determined to be 0.099 mM (HA-Ag), 0.052 mM (HASr2-Ag), and 0.034 mM (HASr3-Ag) at day 5, and 0.269 mM (HA-Ag), 0.135 mM (HASr1-Ag), 0.064 mM (HASr2-Ag), and 0.118 mM (HASr3-Ag) at day 15. The results indicated that after 5 days, the released doses of Ag^+ ions were in the range of previously described MIC (0.094 mM) for silver ion against *S. epidermidis* [25]. The total amounts of silver released from the HA-Ag, HASr1-Ag, HASr2-Ag, and HASr3-Ag bone plates at the end of 15 days were determined to be 98.5%, 52.8%, 26.7%, and 52.1%, respectively. The differences between the release profiles of silver from HASr2-Ag and HASr3-Ag bone plates possibly affect the amount of silver released. Although a similar controlled release profiles of silver from HASr1-Ag and HASr2-Ag bone plates is determined after a small burst release, long-term exposure of silver ions with lower concentrations revealed the sustained release from HASr2-Ag bone plates [Fig. 7(b)]. This result may be due to the amount of Sr incorporated in HA, which may change surface area and release mechanism. The release profiles of Ag^+ form HA-Ag and HASr3-Ag bone plates are similar; however, the results indicate that high concentrations of silver are released from HA-Ag bone plates compared to all. In literature, the toxic effect of Ag^+ ions on osteoblasts or mammalian cells were discussed [25, 54]; nevertheless, these silver-coated HA bone plates need to be investigated further for systemic and long-term toxicity, osseointegration, and their related toxicity to osteoblasts and osteoclasts in vivo.

To evaluate the release mechanisms of Sr^{2+} and Ag^+ from biomimetic coatings, release data were used by several mathematical models (zero order, first order, Higuchi, Hixson–Crowell), and correlation values (R^2) were determined (Table II) from the results of model fitting of the release profiles. As shown in Table II, according to correlation values, Sr^{2+} release data were well fitted to the Higuchi model for HASr1-Ag, HASr2-Ag, and HASr3-Ag coatings, which indicates that Sr^{2+} is released by diffusion [37], The results of model fitting of the Ag^+ release profiles showed higher correlation values for Higuchi model for all the coatings (Table II). However, the best fitting release data of the Hixson–Crowell model for HA-Ag coatings (R^2 = 0.97) suggest that Ag^+ is released from HA-Ag by dissolution, which may be due to the changes in surface area or changes in diameter of particles, and release is not occurred by diffusion [38]. Huang et al. indicated the fact that releasing Ag^+ in the

TABLE II: Mathematical models and parameters based on Sr^{2+} and Ag^+ release data.

	Correlation value (R^2)			
Coating	Zero-order model	First-order model	Higuchi's model	Hixson–Crowell's model
Sr^{2+} release				
HASr1-Ag	0.88	0.81	0.97	0.84
HASr2-Ag	0.94	0.91	0.98	0.92
HASr3-Ag	0.83	0.86	0.94	0.88
Ag^+ release				
HA-Ag	0.93	0.80	0.95	0.97
HASr1-Ag	0.84	0.79	0.91	0.83
HASr2-Ag	0.84	0.78	0.85	0.80
HASr3-Ag	0.90	0.79	0.93	0.85

https://doi.org/10.1557/jmr.2018.447 Published online by Cambridge University Press

© Materials Research Society 2019

initial stage could lead to higher concentrations of Ag^+ in the medium, which could have a bad effect on the osteoblasts [32]. According to their study, they speculated that dual release of Sr^{2+} and Ag^+ might offset the potential cytotoxicity of Ag^+ release. In this study, we concluded that dissolution of Ag^+ from HA coatings could be avoided by the development of HA coating as multilayered biomimetic coatings.

Conclusions

Biomimetic coatings provided by 10× SBF-like solutions revealed an appropriate technique for the fabrication of HASr with a fine control of its strontium content and homogenous Ag coatings were achieved as a second layer on 316L SS bone plates. Results showed that strontium is successfully incorporated into the nano-assembled structure of bone-like apatite by a substitution of Ca^{2+} by Sr^{2+}. Structural and surface properties can be controlled via changing the Sr^{2+} concentration in soaking medium. A controlled and sustained release of Sr^{2+} and Ag^+ provided from HASr1-Ag, HASr2-Ag, and HASr3-Ag bone plates by a release mechanism of diffusion in therapeutically relevant concentrations, which is favorable to exploit dual effect of strontium and silver on bone bonding and antibacterial activity. However, further in vitro and in vivo studies should be carried out to characterize the biological properties of HASr-Ag bone plates and provide further evidence of their potential clinical utility.

Materials and methods

Treatment of bone plates before coating

The 316L SS fracture fixation bone plates were kindly provided by the Department of Orthopedics and Traumatology, Bülent Ecevit University. Before coating the substrates, which are 10 × 10 × 4 mm^3 in size, an alkali treatment was performed as described before [7]. Briefly, samples were soaked in 5 mL of 10 M NaOH aqueous solution at 60 °C for 24 h. Then, they were washed with distilled water and dried at 40 °C for 24 h in an air atmosphere. The alkali-treated substrates were then heated to 500–800 °C at a rate of 5 °C/min in Ni–Cr furnace and cooled to room temperature in the furnace [7].

Coating of HA and HASr on bone plates from 10× SBF by biomimetic HA precipitation (first layer)

SBF solution used in this study has 10 times concentrated calcium and phosphate ions, and biomimetic HA precipitation was carried out using 10× SBF-like solution according to the method of Mavis et al., as described previously [13]. Briefly, the reagent-grade chemicals, purchased from Merck (Darmstadt, Germany), NaCl (58.443 g), KCl (0.373 g), $CaCl_2{\cdot}2H_2O$ (3.675 g), $MgCl_2{\cdot}6H_2O$ (1.016 g), and $NaH_2PO_4{\cdot}H_2O$ (0.250 g), were added into the ultrapure water in the given order to prepare the stock solution. Then, the samples were placed into a beaker of 100 mL of the stock solution. Precipitation was started with the addition of 10 mM $NaHCO_3$ solution, and coating process was achieved at 37 °C for 24 h. Then, HA-coated bone plates were rinsed with distilled water and dried and stored at room temperature.

To prepare strontium-containing HA coatings, first, certain amounts of strontium nitrate [0.025% (w/v), 0.05% (w/v), 0.1% (w/v); Merck, Germany] were added into 100 mL stock solution. Then, the same coating process was performed as mentioned above. Strontium-containing HA-coated bone plates are denoted as HASr1, HASr2, and HASr3 based on their Sr inclusion concentrations of 0.4, 0.8, and 1.6 mM, respectively.

Coating of Ag on biomimetic HA- and HASr-coated bone plates (second layer)

Silver coating of bone plates was performed according to the dip-coating procedure described previously [34]. Polylactic acid (0.2 g; Cargill, Minnetonka, Minnesota) was dissolved in 10 mL of chloroform. About 0.01 mL of the $AgNO_3$ (0.1 M) aqueous solution was added to this solution. Then, HA- and HASr-coated bone plates were dipped into this solution and dried in open air for 5 min. This procedure was repeated 20 times until a fine composite film layer was achieved on the surface of the plates. These film layered plates were dried under vacuum and then put in a furnace at 450 °C for 2 h to diminish the polymer. Thus, silver nanoparticles are adhered to the surface of the biomimetic HA- and HASr-coated bone plates and formed as a second layer on plates. Silver-coated bone plates are denoted as HA-Ag and HASr-Ag.

Characterization of coated bone plates

The structure and morphologies of HA, HASr, HA-Ag, and HASr-Ag coatings on bone plates were investigated by scanning electron microscope (SEM; FEI QUANTA FEG 450, Eindhoven, The Netherlands) at 15 kV under vacuum, and each sample was ion-sputtered with gold prior to examination. For the elemental analysis, the electron microscope was equipped with an energy dispersive X-ray attachment (EDAX/APOLLO X SSD device, Mahwah, NJ). The elemental maps of the prepared samples were investigated for Ca, P, Sr, and Ag. Structural changes and phase purity of the coatings were investigated by X-ray diffraction (XRD; PANalytical Empyrean diffractometer, Royston, United Kingdom; step size: 0.026°, time per step: 99.45 s, scan speed: 0.067°/s, 45 kV–40 mA Cu source). To support the XRD findings of HASr coatings and provide evidence of ionic substitution, Raman spectral characterization of the HASr-coated bone plates was

https://doi.org/10.1557/jmr.2018.447 Published online by Cambridge University Press

© Materials Research Society 2019

performed using a Raman Spectrometer (RENİSHAW Invia, Edge Gloucestershire, United Kingdom) with an excitation wavelength of 532 nm. The composition of the coatings was quantitatively determined by X-ray fluorescence (XRF) on PANalytical equipment (Royston, United Kingdom) with a rhodium tube (4 kW). Therefore, the strontium and silver contents and also the Ca/P ratios could be verified.

In vitro release studies of Sr^{2+} and Ag^{+} from biomimetic bone plates

Sr^{2+} and Ag^{+} release studies from bone plates were performed by incubating bone plates in 10 mL phosphate buffered saline (PBS) solutions (pH = 7.4) at 37 °C. HA-Ag, HASr1-Ag, HASr2-Ag, and HASr3-Ag bone plates were immersed into tubes containing 10 mL PBS. Then, at predetermined time intervals (1, 3, 5, 7, 9, 11, 13, and 15 days), buffer solutions were changed with fresh ones. The amounts of Sr and Ag released from the bone plates were determined at selected time intervals through ICP-OES (PerkinElmer Optima 4300 DV, Wellesley, Massachusetts) analysis, and the cumulative release graphs were maintained.

Mathematical modeling and release kinetics

To investigate the mechanism of Sr^{2+} and Ag^{+} release from biomimetic coated bone plates, in vitro release data were analyzed using various kinetic models. The zero-order kinetic model [Eq. (1)] is described as follows [35]:

$$Q_t = Q_0 + K_0 t \quad , \tag{1}$$

where Q_0 = initial amount of drug, Q_t = cumulative amount of drug release at time "t," and K_0 = zero-order release constant.

The first-order release [Eq. (2)] is defined as follows [36]:

$$\log Q_t = \log Q_0 + K_1 t \quad , \tag{2}$$

where K_1 is the first-order release constant.

Higuchi described the release of drugs from insoluble matrix as a square root of time-dependent process based on the Fickian diffusion [37]:

$$Q_t = Q_0 + K_H t^{1/2} \quad , \tag{3}$$

where K_H is the Higuchi constant.

The Hixson–Crowell cube root law [Eq. (4)] is defined as follows [38]:

$$\sqrt[3]{Q_t} - \sqrt[3]{Q_0} = K_{HC} t \quad , \tag{4}$$

where K_{HC} is the Hixson–Crowell constant.

Modeling was performed using the parameters that provide the closest fit between experimental observations and the nonlinear function. The model that best fits the release data was selected based on the correlation coefficient (R^2) in the models described above. The model that gives the highest R^2 value is considered as the best fit of release data.

Statistical analysis

All data are expressed as means ± standard deviations of a representative of three similar experiments carried out in triplicate.

Acknowledgment

This study was financially supported by Bülent Ecevit University Scientific Research Projects, Project No. 2015-3997 1044-02.

References

1. **T. Hanawa**: Overview of metals and applications. In *Metals for Biomedical Devices* (Woodhead Publishing, Oxford, 2010); pp. 3–24.
2. **F. Bir, H. Khireddine, A. Touati, D. Sidane, S. Yala, and H. Oudadesse**: Electrochemical depositions of fluorohydroxyapatite doped by Cu^{2+}, Zn^{2+}, Ag^{+} on stainless steel substrates. *Appl. Surf. Sci.* **258**, 7021 (2012).
3. **A. Ganser, R.E. Thompson, I. Tami, D. Neuhoff, A. Steiner, and K. Ito**: An in vivo experimental comparison of stainless steel and titanium Schanz screws for external fixation. *Eur. J. Trauma Emerg. Surg.* **59**, 33 (2007).
4. **E.G. Nordström and O.L.S. Muñoz**: Physics of bone bonding mechanism of different surface bioactive ceramic materials in vitro and in vivo. *Biomed. Mater. Eng.* **11**, 221 (2001).
5. **W. Xia, C. Lindahl, J. Lausma, P. Borchardt, A. Ballo, P. Thomsen, and H. Engqvist**: Biomineralized strontium-substituted apatite/titanium dioxide coating on titanium surfaces. *Acta Biomater.* **6**, 1591 (2010).
6. **T.N. Pham, T.M.T. Dinh, T.T. Nguyen, T.P. Nguyen, E. Kergourlay, D. Grossin, G. Bertrand, N. Pebere, S.J. Marcelin, C. Charvillat, and C. Drouet**: Operating parameters effect on physicochemical characteristics of nanocrystalline apatite coatings electrodeposited on 316L stainless steel. *Adv. Nat. Sci.: Nanosci. Nanotechnol.* **8**, 035001 (2017).
7. **F-H. Lina, Y-S. Hsub, S-H. Linb, and J-S. Sun**: The effect of Ca/P concentration and temperature of simulated body fluid on the growth of hydroxyapatite coating on alkali-treated 316L stainless steel. *Biomaterials* **23**, 4029 (2002).
8. **N.R. Babu, S. Manwatkar, K.P. Rao, and T.S.S. Kumar**: Bioactive coatings on 316L stainless steel implants. *Trends Biomater. Artif. Organs* **17**, 43 (2004).
9. **A. Valanezahad, K. Ishikawa, K. Tsuru, M. Maruta, and S. Matsuya**: Hydrothermal calcium modification of 316L stainless

https://doi.org/10.1557/jmr.2018.447 Published online by Cambridge University Press

© Materials Research Society 2019

steel and its apatite forming ability in simulated body fluid. *Dent. Mater. J.* **749**, 30 (2011).

10. **H. Mehboob, M. Awais, H. Khalid, A.A. Ch, S.A. Siddiqi, and I. Rehman**: Polymer-assisted deposition of hydroxyapatite coatings using electrophoretic technique. *Biomed. Eng.* **26**, 1450073 (2014).
11. **T. Kokubo and H. Takadama**: How useful is SBF in predicting in vivo bone bioactivity? *Biomaterials* **27**, 2907 (2006).
12. **A. Oyane, H.M. Kim, T. Furuya, T. Kokubo, T. Miyazaki, and T. Nakamura**: Preparation and assessment of revised simulated body fluids. *J. Biomed. Mater. Res.* **65**, 188 (2003).
13. **B. Maviş, T.T. Demirtaş, M. Gümüşderelioğlu, G. Gündüz, and Ü. Çolak**: Synthesis, characterization and osteoblastic activity of PCL nanofibers coated with biomimetic calcium phosphate. *Acta Biomater.* **5**, 3098 (2009).
14. **C. Wu, J. Chang, W. Zhai, and S. Ni**: A novel bioactive porous bredigite ($Ca_7MgSi_4O_{16}$) scaffold with biomimetic apatite layer for bone tissue engineering. *J. Mater. Sci.: Mater. Med.* **18**, 857 (2007).
15. **T.T. Demirtaş, G. Kaynak, and M. Gümüşderelioğlu**: Bone-like hydroxyapatite precipitated from 10× SBF-like solution by microwave irradiation. *Mater. Sci. Eng., C* **49**, 713 (2015).
16. **E.Ö. Tunçay, T.T. Demirtaş, and M. Gümüşderelioğlu**: Microwave-induced production of boron-doped HAp (B-HAp) and B-HAp coated composite scaffolds. *J. Trace Elem. Med. Biol.* **40**, 72 (2017).
17. **S.G. Dahl, P. Allain, P.J. Marie, Y. Mauras, G. Boivin, P. Ammann, Y. Tsouderos, P.D. Delmas, and C. Christiansen**: Incorporation and distribution of strontium in bone. *Bone* **28**, 446 (2001).
18. **P.J. Marie**: Optimizing bone metabolism in osteoporosis: Insight into the pharmacologic profile of strontium ranelate. *Osteoporosis Int.* **14**, 9 (2003).
19. **I. Pereiro, C. Rodriguez-Valencia, C. Serra, E.L. Solla, J. Serra, and P. Gonzalez**: Pulsed laser deposition of strontium-substituted hydroxyapatite coatings. *Appl. Surf. Sci.* **258**, 9192 (2012).
20. **A.R. Boyd, L. Rutledge, L.D. Randolph, and B.J. Meenana**: Strontium-substituted hydroxyapatite coatings deposited via a co-deposition sputter technique. *Mater. Sci. Eng., C* **46**, 290 (2015).
21. **C.T. Wong, W.W. Lu, W.K. Chan, K.M. Cheung, K.D. Luk, D. S. Lu, A.B. Rabie, L.F. Deng, and J.C. Leong**: In vivo cancellous bone remodeling on a strontium-containing hydroxyapatite (Sr-HA) bioactive cement. *J. Biomed. Mater. Res.* **68A**, 513 (2004).
22. **G.X. Ni, W.W. Lu, K.Y. Chiu, Z.Y. Li, D.Y. Fong, and K.D. Luk**: Strontium-containing hydroxyapatite (Sr-HA) bioactive cement for primary hip replacement: An in vivo study. *J. Biomed. Mater. Res., Part B* **77**, 409 (2006).
23. **W. Xia, C. Lindahl, J. Lausmaa, P. Borchardt, A. Ballo, P. Thomsen, and H. Engqvist**: Biomineralized strontium-substituted apatite/titanium dioxide coating on titanium surfaces. *Acta Biomater.* **6**, 1591 (2010).
24. **W. Xue, H.L. Hosick, A. Bandyopadhyay, S. Bose, C. Ding, K.D. K. Luk, K.M.C. Cheung, and W.W. Lu**: Preparation and cell-materials interactions of plasma sprayed strontium-containing hydroxyapatite coating. *Surf. Coat. Technol.* **201**, 4685 (2007).
25. **C.E. Albers, W. Hofstetter, K.A. Siebenrock, R. Landmann, and F.M. Klenke**: In vitro cytotoxicity of silver nanoparticles on osteoblasts and osteoclasts at antibacterial concentrations. *Nanotoxicology* **7**, 30 (2013).
26. **A. Melaiye and W.J. Youngs**: Silver and its application as an antimicrobial agent. *Expert Opin. Ther. Pat.* **15**, 125 (2005).
27. **C.S. Ciobanu, F. Massuyeau, L.V. Constantin, and D. Predoi**: Structural and physical properties of antibacterial Ag-doped nano-hydroxyapatite synthesized at 100 °C. *Nanoscale Res. Lett.* **613**, 1 (2011).
28. **Q.L. Feng, T.N. Kim, J. Wu, E.S. Park, J.O. Kim, D.Y. Lim, and F.Z. Cui**: Antibacterial effects of Ag-HAp thin films on alumina substrates. *Thin Solid Films* **335**, 214 (1998).
29. **W. Chen, Y. Liu, H.S. Courtney, M. Bettenga, C.M. Agrawal, J.D. Bumgardner, and J.L. Ong**: In vitro anti-bacterial and biological properties of magnetron co-sputtered silver-containing hydroxyapatite coating. *Biomaterials* **27**, 5512 (2006).
30. **M. Mirzaee, M. Vaezi, and Y. Palizdar**: Synthesis and characterization of silver doped hydroxyapatite nanocomposite coatings and evaluation of their antibacterial and corrosion resistance properties in simulated body fluid. *Mater. Sci. Eng., C* **69**, 675 (2016).
31. **G.A. Fielding, M. Roy, A. Bandyopadhyay, and S. Bose**: Antibacterial and biological characteristics of plasma sprayed silver and strontium doped hydroxyapatite coatings. *Acta Biomater.* **8**, 3144 (2012).
32. **Y. Huang, X. Zhang, H. Zhang, H. Qiao, X. Zhang, T. Jia, S. Han, Y. Gao, H. Xiao, and H. Yang**: Fabrication of silver- and strontium-doped hydroxyapatite/TiO_2 nanotube bilayer coatings for enhancing bactericidal effect and osteoinductivity. *Ceram. Int.* **43**, 992 (2017).
33. **Z. Geng, R. Wang, X. Zhuo, Z. Li, Y. Huang, and L. Ma**: Incorporation of silver and strontium in hydroxyapatite coating on titanium surface for enhanced antibacterial and biological properties. *Mater. Sci. Eng., C* **71**, 852 (2017).
34. **D.B. Hazer, M. Sakar, Y. Dere, G. Altinkanat, M.I. Ziyal, and B. Hazer**: Antimicrobial effect of polymer-based silver nanoparticle coated pedicle screws—experimental research on biofilm inhibition in rabbits. *Spine* **41**, 323 (2016).
35. **T.P. Hadjiioannou, G.D. Christian, M.A. Koupparis, and P. E. Macheras**: *Quantitative Calculations in Pharmaceutical Practice and Research* (VCH Publishers, New York, New York, 1993).
36. **D.W.A. Bourne**: Pharmacokinetics. In *Modern Pharmaceutics* (Marcel Dekker, New York, New York, 2002); pp. 67–93.
37. **T. Higuchi**: Mechanism of sustained-action medication. Theoretical analysis of rate of release of solid drugs dispersed in solid matrices. *J. Pharm. Sci.* **52**, 1145 (1963).
38. **A.W. Hixson and J.H. Crowell**: Dependence of reaction velocity upon surface and agitation. *Ind. Eng. Chem.* **23**, 923 (1931).

https://doi.org/10.1557/jmr.2018.447 Published online by Cambridge University Press

© Materials Research Society 2019

39. **D.S. Tavares, C.X. Resende, M.P. Quitan, L.O. Castro, J.M. Granjeiro, and G.A. Soares**: Incorporation of strontium up to 5 mol. (%) to hydroxyapatite did not affect its cytocompatibility. *Mater. Res.* **14**, 456 (2011).
40. **G.S. Mandair and M.D. Morris**: Contributions of Raman spectroscopy to the understanding of bone strength. *BoneKEy Rep.* **4**, 620 (2015).
41. **M. Quade, M. Schumacher, A. Bernhardt, A. Lode, M. Kampschulte, A. Voß, P. Simon, O. Uckermann, M. Kirsche, and M. Gelinsky**: Strontium-modification of porous scaffolds from mineralized collagen for potential use in bone defect therapy. *Mater. Sci. Eng., C* **84**, 159 (2018).
42. **A. Bigi, E. Boanini, C. Capuccini, and M. Gazzano**: Strontium-substituted hydroxyapatite nanocrystals. *Inorg. Chim. Acta* **360**, 1009 (2007).
43. **M.D. O'Donnell, Y. Fredholm, A. de Rouffignac, and R.G. Hill**: Structural analysis of a series of strontium-substituted apatites. *Acta Biomater.* **4**, 1455 (2008).
44. **T.S.B. Narasaraju and D.E. Phebe**: Some physico-chemical aspects of hydroxylapatite. *J. Mater. Sci.* **33**, 1 (1996).
45. **E. Canalis, M. Hott, P. Deloffre, Y. Tsouderos, and P.J. Marie**: The divalent strontium salt S12911 enhances bone cell replication and bone formation in vitro. *Bone* **18**, 517 (1996).
46. **C. Chang, C. Tu, T.H. Chen, L. Komuves, Y. Oda, S.A. Pratt, S. Miller, and D. Shoback**: Expression and signal transduction of calcium-sensing receptors in cartilage and bone. *Endocrinology* **140**, 5883 (1999).
47. **A. Barbara, P. Delannoy, B. Denis, and P. Marie**: Normal matrix mineralization induced by strontium ranelate in MC3T3-E1 osteogenic cells. *Metabolism* **53**, 532 (2004).
48. **J. Braux, F. Velard, C. Guillaume, S. Bouthors, E. Jallot, J-M. Nedelec, D. Laurent-Maquin, and P. Laquerrière**: A new insight into the dissociating effect of strontium on bone resorption and formation. *Acta Biomater.* **7**, 2593 (2011).
49. **M. Schumacher, A. Lode, A. Helth, and M. Gelinsky**: A novel strontium(II)-modified calcium phosphate bone cement stimulates human-bone-marrow-derived mesenchymal stem cell proliferation and osteogenic differentiation in vitro. *Acta Biomater.* **9**, 9547 (2013).
50. **C. O'Sullivan, P. O'Hare, N.D. O'Leary, A.M. Crean, K. Ryan, A.D. W. Dobson, and L. O'Neill**: Deposition of substituted apatites with anticolonizing properties onto titanium surfaces using a novel blasting process. *J. Biomed. Mater. Res., Part B* **95B**, 141 (2010).
51. **F. Yang, D. Yang, J. Tu, Q. Zheng, L. Cai, and L. Wang**: Strontium enhances osteogenic differentiation of mesenchymal stem cells and in vivo bone formation by activating Wnt/catenin signaling. *Stem Cells* **29**, 981 (2011).
52. **O. Gordon, T.V. Slenters, P.S. Brunetto, A.E. Villaruz, D. E. Sturdevant, and M. Otto**: Silver coordination polymers for prevention of implant infection: Thiol interaction, impact on respiratory chain enzymes, and hydroxyl radical induction. *Antimicrob. Agents Chemother.* **54**, 4208 (2010).
53. **G. Gosheger, J. Hardes, H. Ahrens, A. Streitburger, H. Buerger, and M. Erren**: Silver-coated megaendoprostheses in a rabbit model—an analysis of the infection rate and toxicological side effects. *Biomaterials* **25**, 5547 (2004).
54. **D. Langanki, M.E. Ogle, J.D. Cameron, R.A. Lirtzman, R. E. Schroeder, and M.W. Mirsch**: Evaluation of a novel bioprosthetic heart valve incorporating anticalcification and antimicrobial technology in a sheep model. *J. Heart Valve Dis.* **7**, 633 (1998).

https://doi.org/10.1557/jmr.2018.447 Published online by Cambridge University Press

© Materials Research Society 2019